Fuel 295 (2021) 120509

Contents lists available at ScienceDirect

Fuel

journal homepage: www.elsevier.com/locate/fuel

Property predictions demonstrate that structural diversity can improve the performance of polyoxymethylene ethers as potential bio-based diesel fuels

Danielle L. Bartholet [a], Martha A. Arellano-Treviño [c], Fan Liang Chan [b], Stephen Lucas [b], Junqing Zhu [d], Peter C. St. John [c], Teresa L. Alleman [c], Charles S. McEnally [d], Lisa D. Pfefferle [d], Daniel A. Ruddy [c], Bret Windom [b], Thomas D. Foust [b,c], Kenneth F. Reardon [a,b,*]

[a] Colorado State University, Department of Chemical and Biological Engineering, Campus Delivery 1370, Fort Collins, CO 80523-1370, USA
[b] Colorado State University, Department of Mechanical Engineering, Campus Delivery 1374, Fort Collins, CO 80523-1374, USA
[c] National Renewable Energy Laboratory, Catalytic Carbon Transformation & Scale-up Center, 15013 Denver West Parkway, Golden, CO 80401, USA
[d] Yale University, Department of Chemical and Environmental Engineering, 9 Hillhouse Avenue, New Haven, CT 06520, USA

ARTICLE INFO

Keywords:
Oxygenate
Polyoxymethylene ether
Diesel blendstock
Fuel property predictions
Soot formation
Biofuel

ABSTRACT

High emissions of particulate matter from diesel engines presents a serious risk to human health and the environment. The addition of oxygenated molecules to diesel fuels has been shown to reduce soot formation during combustion. Polyoxymethylene ethers (POMEs) are a novel class of oxygenated molecules that can be produced from biomass and that have the potential to be used as soot-reducing diesel fuel blendstocks. However, only a few variations of these molecules have been studied thus far, and those that have been characterized present significant disadvantages that could compromise current liquid fuel systems and diesel engines. Using a variety of structure–activity models, we evaluated 67 POMEs to predict the effects of structural variations on important fuel properties. Prediction accuracy was assessed by comparing predictions with measurements for a subset of structures. Nine POME molecules were identified as having potential to reduce soot formation by over 75% compared to conventional diesel fuels while being compatible with current liquid fuel infrastructure, maintaining optimal engine performance, and presenting a minimal risk to the environment. None of these nine POMEs has been previously identified as a potential diesel blendstock. This is the first evaluation of POMEs as a class of molecules and the results guide research on the synthesis, properties, and engine performance of POMEs.

1. Introduction

Compression ignition (CI) engines provide the benefit of improved efficiency when compared to spark ignition engines. However, the combustion of diesel fuels in CI engines produces more particulate matter (PM) than the combustion of gasoline in spark ignition engines [1]. Adverse effects on climate change and human health have been linked to PM from fossil fuel combustion [2–5]. Jacobson reported that PM is the second-most significant contributor to global warming following carbon dioxide [2,6]. Also concerning are the well-documented short and long-term effects of PM on pulmonary and cardiovascular health, leading to millions of premature deaths [3–5,7,8]. While novel, alternative fuels and propulsion system designs are important technologies to investigate as long-term solutions to the problems created by fossil fuel dependence, massive changes in energy infrastructure are not likely to occur for many years. Therefore, solutions must be found to minimize the ecological and health impacts of diesel fuel combustion within the current infrastructure. A promising solution is the rational design of environmentally benign diesel fuel blendstocks that will reduce PM emissions while maintaining or improving engine efficiency.

Many studies have investigated the effects of oxygenated fuel blendstocks on the formation of PM during diesel combustion [9–15]. The presence of carbon–oxygen bonds leads to lower concentrations of the soot precursors that are formed in the locally fuel-rich premixed ignition that is characteristic of diesel engines [10]. However, the presence of oxygen has a negative impact on the lower heating value (LHV) of a fuel component. While soot reduction depends on oxygen content to the first order [16], it also depends on the specific oxygenated functionality [17] so the molecular structures and physicochemical

* Corresponding author at: Colorado State University, Department of Chemical and Biological Engineering, Campus Delivery 1370, Fort Collins, CO 80523-1370, USA.
E-mail address: Kenneth.Reardon@colostate.edu (K.F. Reardon).

https://doi.org/10.1016/j.fuel.2021.120509
Received 21 December 2020; Received in revised form 13 February 2021; Accepted 15 February 2021
Available online 19 March 2021

properties of the oxygenated species are important when considering blending effects and engine performance. For example, ethanol is commonly added to gasoline, but its use as a diesel fuel additive is limited by low cetane number; low flashpoint temperature, which creates headspace flammability concerns in fuel tanks; and poor miscibility, which results in the need for engine and distribution infrastructure modifications [11,12,18].

It is also important to consider the environmental fate of a potential fuel additive molecule. Methyl *tert*-butyl ether (MTBE) was used widely as an oxygenated additive in gasoline to reduce emissions. However, due to its water solubility and environmental persistence, MTBE became a problematic groundwater and soil contaminant [19] and is no longer used as a fuel additive in the United States [20].

A molecule that has recently gained attention as a potential diesel additive is dimethoxymethane (DMM), also known as methylal (Fig. 1). DMM has been shown to significantly reduce soot [21]; however, it has a much lower LHV than petroleum fuels, is highly soluble in water, and fails to meet the diesel criteria for flash point (T_{flash}). Recently, polyoxymethylene dimethyl ethers (POMDMEs), molecules similar to DMM but with longer oxymethylene backbones, have been investigated [21–25] (Fig. 2). The increased oxygen content of POMDMEs suggests they would provide effective suppression of soot formation, and POMDMEs of backbone length n = 2–3 (Fig. 2) may be more miscible in diesel fuel [22] and have higher cetane numbers than DMM. However, due to the high oxygen content and short alkyl end groups of POMDMEs, they have low LHV and are likely to be highly water soluble and non-biodegradable, making them potential environmental contaminants. Lautenschütz et al. also investigated the fuel properties of POMDME analogs that have ethyl end groups [26]. While these ethyl-terminated polyoxymethylene ethers (POMEs) demonstrated some favorable properties, such as high cetane numbers, they still fell short of optimal LHVs for diesel fuel [26]. Furthermore, that study did not consider whether the investigated POMEs could be potential environmental contaminants.

Industrially, DMM, (MM-$POME_1$; see Section 2.1 for nomenclature) is synthesized by acetalization of formaldehyde [21]. Chain propagation can then be achieved through reacting paraformaldehyde and MM-$POME_1$ over an acid catalyst to produce POMDMEs (MM-$POME_2$ through MM-$POME_8$). These methyl-terminated POMEs have also been synthesized directly from dimethyl ether over a $Ti(SO_4)_2$/activated carbon catalyst with high selectivity [27]. Current research is focused on improving the synthesis of POMEs [28], so it is vital to identify which molecules have the potential to be industrially valuable. All of these routes can use biomass as the starting feedstock so that the produced POMEs can be renewable, low-carbon biofuels.

In this study, we used a rational design approach to identify POMEs with the potential to reap the benefits of POMDMEs, including effective soot reduction and high cetane number, while circumventing the limitations of engine and infrastructure incompatibility and environmental concerns. Sixty-seven candidate POMEs (Fig. 3) were evaluated, including linear structures of backbone length n = 1–7 and alkyl end groups of length C1-C5 as well as structures with isopropyl and isobutyl end groups, and structures with a tertiary alkyl branch of length C1-C4. Only a few variants of POMEs have been investigated previously, and most of their fuel properties remain unknown. Thus, several predictive tools were used to estimate the LHV, melting point (T_{melt}), T_{flash}, biodegradability, water solubility, ignition delay, derived cetane number (DCN), and hydrocarbon solubility of each molecule. There is no ASTM standard test for characterizing the sooting tendency of diesel fuels, so most fuel design studies are unable to consider soot (e.g., [29]). In this study we include soot by using a relatively new parameter, yield

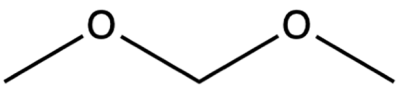

Fig. 1. Chemical structure of dimethoxymethane (DMM).

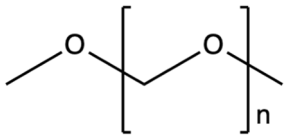

Fig. 2. General chemical structure of polyoxymethylene dimethyl ethers (POMDMEs).

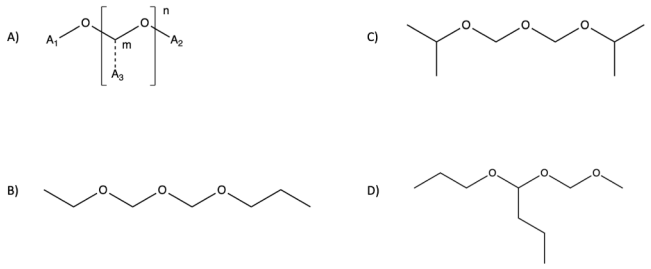

Fig. 3. Polyoxymethylene ether (POME) structures. (A) General structure of POMEs. A_1, A_2, and A_3 are alkyl terminating groups, and *n* is the POME backbone length. The possible single branch point is indicated at *m*, and the dotted line indicates that some POME molecules are not branched. (B) Example of linear POME with linear end groups: EP-$POME_2$. (C) Example of linear POME with branched end groups: iPiP-$POME_2$. (D) Example of branched POME with linear end groups: 1P-PM-$POME_2$. Only structures with a single A_3 group were considered in this study.

sooting index (YSI), which is defined as the amount of soot formed by a fuel when it is doped at low concentration into a base methane/air flame [49]. We have shown elsewhere that YSI correlates well with the ASTM D1322 smoke point test used for characterizing sooting tendencies of jet fuels but has the benefit of requiring less sample volume (100 μL vs 10 mL) and offering a wider dynamic range that encompasses low soot molecules such as POMEs [30,31]. POMEs were evaluated against fuel criteria both as pure compounds and as blendstocks in diesel fuel at 10–50% blending.

2. Materials and methods

2.1. POME nomenclature

A general nomenclature for POMEs is defined here as *mA3- A1A2-POMEn*, where A_1 and A_2 represent the terminating alkyl groups and A_3 represents an optional tertiary branch. Alkyl groups are designated by M, E, P, B, and Pe for methyl, ethyl, propyl, butyl, and pentyl groups respectively. The branch point (if present) is indicated by *m*, and *n* is the POME backbone length (Fig. 3A). Linear POMEs (Fig. 3B) are named by ordering the terminating groups from shortest to longest. POMEs with *iso*-alkyl groups were also considered and are denoted as iP or iB for isopropyl and isobutyl groups respectively (Fig. 3C). The first term of the general nomenclature accounts for tertiary branching (Fig. 3D). When naming branched POMEs, the branch point, m, is numbered from the closer end and the terminating groups named beginning with that end.

2.2. Pomes used in property measurements

MM-$POME_1$ (DMM; 99.0% from Sigma-Aldrich and 99.5% from Acros), EE-$POME_1$ (ethylal; 99.0% from Acros and 99.0% from Merck), and BB-$POME_1$ (butylal; 98.5% from Sigma-Aldrich) were used as received. A mixture of $POME_{3-6}$ was procured from ASG Analytik-Service GmbH (Germany). The mixture was fractionated and purified via distillation (spinning band) to obtain MM-$POME_3$, MM-$POME_4$, MM-$POME_5$, and MM-$POME_6$.

2.3. Estimation of POME properties

2.3.1. Boiling point, melting point, and flash point

Basic physical properties such as melting point and boiling point were considered to ensure that the blendstock can be handled within the existing liquid fuel infrastructure and can be blended and combusted easily with diesel fuels. Melting point is an important property when considering the engine compatibility and cold- flow properties of a potential fuel additive. At temperatures below the melting point, crystallization can occur, leading to improper fuel delivery and injection resulting in poor combustion [32]. Criteria for low temperature properties are typically specified regionally based on local ambient conditions (ASTM D975-20a) [33].

Since diesel fuel is a highly complex multicomponent mixture, the boiling point (T_{boil}) is specified as the 90% distillation temperature, T90. To ensure that blending with POMEs will not affect the T90 of diesel fuels, the T_{boil} values of pure POMEs must be considered. The flash point is an indicator of flammability and is important for safe transportation, storage, and use of a fuel [34]. It was therefore considered to ensure safe handling and transportation of both the pure POME and the finished fuel blend as well as behavior within existing diesel engines.

The Estimation Programs Interface Suite (EPI Suite) software [35] was used to predict T_{boil} from the Adapted Stein and Brown Method, and T_{melt} (Mean or Weighted T_{melt}). T_{flash} values were then calculated from the predicted boiling points using three models: Butler [36] (Eqn. (1)), Prugh [37] (Eqn. (2)), and Prugh alcohol [37] (Eqn. (3)). The Prugh and Prugh alcohol models also depend on elemental mass percentages through the parameter X_{st} (Eqn. (4)). Measured flash points were used to select the most appropriate T_{flash} model.

$$T_{flash}(^{\circ}F) = 0.683 \cdot T_{boil}(^{\circ}F) - 119 \tag{1}$$

$$T_{flash}(K) = \frac{T_{boil}(K)}{1.442 - 0.08512 \cdot \ln(X_{st})} \tag{2}$$

$$T_{flash}(K) = \frac{T_{boil}(K)}{1.3611 - 0.0697 \cdot \ln(X_{st})} \tag{3}$$

$$X_{st} = \frac{83.8}{4.0 \cdot C + 4.0 \cdot \mathrm{S} + \mathrm{H} - \mathrm{X} - 2.0 \cdot \mathrm{O} + 0.84} \tag{4}$$

In Equation (4), C, O, H, and S represent the elemental mass percentages of carbon, oxygen, hydrogen, and sulfur in the candidate molecule, and X represents the elemental mass percentage of halogens.

2.3.2. Lower Heating Value

LHV is an important property for efficiency and fuel economy, so POMEs with higher LHVs are desirable. Three models were used to predict higher heating values (HHV) for each candidate molecule: The Dulong equation [38] (Eqn. (5)), the Boie model [39] (Eqn. (6)), and the Lloyd and Davenport model [40] (Eqn. (7)). Each uses the elemental mass percentages of carbon, oxygen, hydrogen, nitrogen, and sulfur [38–41]. Lower heating values (LHV) were then calculated according to ASTM D240 [42] (Eqn. (8)). Measured LHV values for several POMEs were used to select the most appropriate model.

$$HHV\left(\frac{MJ}{kg}\right) = 0.336 \cdot C + 1.418 \cdot H + 0.094 \cdot S - 0.145 \cdot O \tag{5}$$

$$HHV\left(\frac{MJ}{kg}\right) = 0.3515 \cdot C + 1.1617 \cdot H + 0.06276 \cdot N + 0.1046 \cdot S - 0.1109 \cdot O \tag{6}$$

$$HHV\left(\frac{MJ}{kg}\right) = 0.3578 \cdot C + 1.1357 \cdot H + 0.059 \cdot N + 0.1119 \cdot S - 0.0845 \cdot O \tag{7}$$

$$LHV\left(\frac{MJ}{kg}\right) = HHV - 0.2122 \cdot H \tag{8}$$

2.3.3. Yield Sooting Index

The YSI, an index of sooting tendency, was evaluated to identify clean-burning molecules predicted to have low propensity for soot formation. YSI was predicted using a group contribution model for sooting tendency [43]. For the predictions reported here, the model used a training set consisting of about 500 measured YSIs for regular hydrocarbons and oxygenates.

2.3.4. Derived Cetane Number and Ignition Delay

Ignition delay (τ) and DCN are important metrics to evaluate combustion speed and fuel quality. These properties were evaluated to ensure that POMEs will not compromise the engine performance of blended fuels. Here, the ignition delay is defined as time following injection before primary heat release from autoignition of the fuel, thus accounting for both the mixture formation and ignition chemical kinetics. Values of τ were calculated from a group contribution model [44] using predicted vapor pressures and molecular structures. The EPI Suite software [35] was used to predict vapor pressures as the mean of the Antoine and Grain methods. The ignition delay is then typically used to calculate DCN from ASTM D6890 [45] (Eqn. (9)–(10)).

$$DCN = 4.460 + \frac{186.6}{\tau} \qquad 3.1ms \le \tau \le 6.5ms \tag{9}$$

$$DCN = 83.99(\tau - 1.512)^{-0.658} + 3.547 \qquad \text{Otherwise} \tag{10}$$

For many of the candidate POME molecules, the calculated ignition delays were <1.512 ms and thus the DCN could not be calculated from Eqs. (9) and (10).

A machine learning model was also used to predict DCN. The model was trained using a previously developed database of nearly 500 cetane measurements from both IQT-based DCN and CFR engine CN tests [46]. The model takes the form of a graph neural network, where a molecule's structure is encoded in a graph consisting of atoms (nodes) and bonds (edges), each with distinct features [47]. In this model, atom features included the element type, total number of attached hydrogens, aromaticity, and presence in a ring. Bond features included the element type of the bridged atoms, bond type, and presence in a ring. After training, the model reached a mean absolute error on held-out validation data of 8.02 CN units. Predictions reported here were taken from the September 29th, 2020 version of the model.

2.3.5. Biodegradability and Water Solubility

Biodegradability and water solubility were evaluated to determine the potential for detrimental persistence in the environment. In the handling and distribution of liquid fuels, the release of small amounts of these fuels into the environment is inevitable, and molecules that are highly soluble will easily enter ground and surface water. Therefore, it is important that all fuel components will biodegrade into non-toxic, environmentally benign products.

The Ready Biodegradability Prediction from the EPI Suite [35] BIOWIN model, which accounts for both aerobic and anaerobic biodegradation, was used for biodegradability assessment. Water solubility was predicted from the EPI Suite model based on the octanol/water partition coefficient. The solubility of MTBE, used to determine the criterion for POME solubility, was also predicted using EPI Suite due to the variability of published data and to provide a consistent comparison to predicted POME solubilities.

2.3.6. Solubility in hydrocarbons

Solubility in hydrocarbons is a critical parameter for miscibility with hydrocarbon-based fuels [48]. The first level of a group contribution method [49] was used to estimate Hansen Solubility Parameters for

dispersion (δ_d), polarity (δ_p), and hydrogen bonding (δ_{hb}). Solubility parameters for conventional diesel fuel were found in the literature [50]. The sphere of solubility was determined by using the solubility of n-butanol in diesel as a limit, where the radius, R, is equivalent to the distance between diesel fuel and n-butanol on the Hansen solubility diagram. The solubility parameters for butanol and ethanol were also found in the literature [50]. The sphere of solubility is given by:

$$\left(\delta_d - \delta_{d,diesel}\right)^2 + \left(\delta_p - \delta_{p,diesel}\right)^2 + \left(\delta_{hb} - \delta_{hb,diesel}\right)^2 = R^2 \quad (11)$$

where

$\delta_{d,diesel} = 14.51$

$\delta_{d,butanol} = 16.0$

$\delta_{p,diesel} = 3.18$

$\delta_{p,butanol} = 7.5$

$\delta_{hb,diesel} = 5.79$

$\delta_{hb,butanol} = 15.8$

and

$$R = \sqrt{\left(\delta_{d,butanol} - \delta_{d,diesel}\right)^2 + \left(\delta_{p,butanol} - \delta_{p,diesel}\right)^2 + \left(\delta_{hb,butanol} - \delta_{hb,diesel}\right)^2}$$

2.4. Estimation of POME-Diesel blend properties

2.4.1. Flash point estimation

Wickey and Chittenden [51] proposed a simple method for calculating flash points of mixtures ($T_{flash,mix}$) that depends only on the flash point ($T_{flash,i}$) and volume fractions (φ_i) of the components (i) (Eqn. (12)–(14)).

$$log_{10}\ (I_i) = -6.1188 + \frac{2414}{T_{flash,i}(^\circ C) + 230.56} \quad (12)$$

$$I_{mix} = \sum \varphi_i I_i \quad (13)$$

$$T_{flash,mix}(^\circ C) = \frac{2414}{6.1188 + log_{10}(I_{mix})} - 230.56 \quad (14)$$

2.4.2. LHV estimation

Several studies have demonstrated that the LHV of a mixture is linearly dependent on the blendstock fraction [52,53]. Tesfa et al. [52] proposed Equation (15) for estimating the LHV of biodiesel blended diesel fuels as a function of the blendstock volume fraction X:

$$LHV_{blend} = -0.041X + 42.32 \quad (15)$$

Here, we use a simple linear mixing rule based on the LHV of each of the components (LHV_i):

$$LHV_{blend} = \sum X_i LHV_i \quad (16)$$

2.4.3. YSI Estimation

McEnally et al. [54] showed that a linear mixing rule (Eqn. (17)) is accurate for predicting YSI based on the YSI of each component (YSI_i).

$$YSI_{blend} = \sum X_i YSI_i \quad (17)$$

Here, X_i is the blendstock mole fraction and YSI_i is the YSI of each component. The YSI of certification diesel fuel was measured as 256 in this study. The molecular weight of the V2 diesel surrogate was used as an estimate for the molecular weight of diesel fuel [55].

2.5. Screening POMEs as potential diesel blendstocks

The process of screening POME molecules involved two phases, the first of which addresses basic requirements for a diesel fuel (Table 1). The POMEs passing the first screening phase were then evaluated for properties desirable to produce a clean-burning fuel (Table 2).

The criteria for boiling point and flash point were determined based on ASTM standards for conventional (No. 2-D) diesel fuel. Thus, the ASTM T90 limit for diesel fuel, as 338 °C, was established as the boiling point criterion for POMEs. Also stated in ASTM D975-20a [33], No.2-D diesel fuels are required to have a flash point above 52 °C. ASTM D975 does not specify a cloud point criterion, which depends on the ambient temperature where the finished blend will be used. While cloud point is a widely used metric to evaluate cold weather operability, no models for cloud point estimation are available. Therefore, melting point was used to evaluate the cold flow properties of POMEs. The criterion of 0 °C for the blendstock melting point was selected to ensure acceptable operability in most conditions and handling in liquid fuel infrastructures. Blendstocks with lower melting points would likely be required seasonally in some regions.

There is no ASTM specification for the LHV of diesel fuels. Therefore, to develop an LHV criterion, a comparison was made to ethanol-blended gasoline. Ethanol is commonly blended into gasoline with a blendstock fraction of 10% and has a low LHV of 28.89 ± 0.3 MJ/kg [56]. The LHV of 10% ethanol blended gasoline (E10 gasoline) is 3.9% lower (43.95 ± 0.60) [56] than that of gasoline without ethanol (45.72 ± 0.20). Since this small reduction of LHV is widely accepted for gasoline, the criterion for LHV of pure POMEs has been specified so that the LHV of 10% POME-diesel blends is no more than>3.9% lower than that of conventional diesel (43 MJ/kg) [53].

DCN was predicted as an indicator of combustion speed. The No.2-D diesel cetane number required by ASTM D975 [33] was used as the criterion for pure POMEs.

The solubility of n-butanol in diesel fuel [50] was used to determine the acceptable radius of solubility (R, Eqn. (11)) for POMEs in diesel, meaning that molecules will need to be more soluble than butanol in diesel fuel to meet this criterion. This limit was chosen for R because butanol has been studied as a diesel blendstock and demonstrates acceptable diesel solubility [57].

The ratio YSI/LHV was used to evaluate the sooting tendency as a function of energy output per kilogram of fuel. The limit for this criterion was calculated by using a maximum YSI of 64 and a minimum LHV of 26.5 MJ/kg as described above. The YSI limit of 64 is 75% lower than the value (YSI = 246) that was measured for a certification diesel fuel using the procedures in Section 2.6.2. This diesel fuel sample is described by Mueller et al. [55] and it was assumed to have the same formula and molecular weight ($C_{13.2}H_{23.0}$; 181.4 g/mol) as the V2

Table 1
Phase 1 screening criteria: fuel property focus.

Property	Requirement	Description/ Significance	Reference/ Justification
Boiling point	<338 °C	Blendstock must boil below the T90 limit for conventional diesel	ASTM D975-20a
Melting point	<0 °C	Cold weather operability	ASTM D975-20a
Flash point	>52 °C	Safety of handling blendstock and finished fuel	ASTM D975-20a
LHV	>26.5 MJ/kg	Fuel economy	Less LHV penalty than E_{10} gasoline
DCN	> 40	Indicator of combustion speed	ASTM D975-20a ASTM D6890
Solubility in diesel	R < 10.26 relative to conventional diesel	Blendstock must be soluble in conventional diesel fuel	More soluble than n-butanol

Table 2
Phase 2 screening criteria: environmental focus.

Property	Requirement	Description/ Significance	Reference/ Justification
YSI/LHV	<2.415 kg/MJ	Prevent soot formation in combustion	YSI 75% below the YSI of diesel. LHV criterion as defined in Phase 1.
Environmental fate	If non-biodegradable, water solubility must be <1980 mg/L	Prevent environmental contamination	Non-biodegradable molecules must be 10 times less soluble than MTBE

surrogate defined in that work [55]. Water solubility and biodegradability were combined into one metric to evaluate the potential for environmental contamination. Molecules that are predicted not to be biodegradable must be at least one order of magnitude less soluble in water than MTBE, which has a predicted solubility of 19,800 mg/L [35] in water. Highly soluble molecules that are predicted to be readily biodegradable pass this screen.

2.6. Measurement of POME properties

2.6.1. LHV

The HHV of the purchased/purified POMEs with alkyl group of C1 or greater (MM-POME$_1$, EE-POME$_1$, and BB-POME$_1$) were determined using an IKA-C200 calorimeter. Approximately 1.0 g of sample was used in each measurement. Measurements were conducted with the bomb calorimeter under excess pure oxygen at 3.0 MPa. The LHV was then calculated using Equation (8).

2.6.2. YSI

The sooting tendencies of the POMEs were measured using our yield-based approach [58]. The specific procedures and apparatus used in this study are described in McEnally et al. [54]. The procedure consisted of three steps: (1) we sequentially doped 1000 ppm of n-heptane, toluene, and each POME into the fuel of a nitrogen-diluted methane flame; (2) we measured the maximum soot concentration in each flame with line-of-sight spectral radiance (LSSR); and (3) we rescaled the measured signals into YSI values using:

$$YSI_{POME} = (YSI_{TOL} - YSI_{HEP}) \times \frac{LSSR_{POME} - LSSR_{HEP}}{LSSR_{TOL} - LSSR_{HEP}} + YSI_{HEP} \quad (18)$$

where the subscripts POME, TOL, and HEP refer to the test POME, toluene, and n-heptane. This rescaling method factors out many sources of systematic uncertainty such as errors in the gas-phase reactant flowrates. Furthermore, it allows the new results to be quantitatively compared with a database [59] that contains measured YSIs for hundreds of organic compounds. The parameters YSI_{TOL} and YSI_{HEP} are constants that define the YSI scale; their values—170.9 and 36.0—were taken from the database so that the newly measured YSIs would be on the same scale. The YSI for each POME was measured three times. Isooctane was used as an internal standard and its YSI was measured 10 times over the course of this study. The values were consistent over time, their average (63.2) agreed with earlier studies (61.7), [43] and their standard deviation was 1.2%. For compounds with very low YSIs – including all of the POMEs in this study – the overall uncertainty is ±5 YSI units [54] This estimate includes random uncertainty based on two standard deviations of the YSI measured for the internal standard and systematic uncertainty due to possible errors in the dopant mass densities that were used to calculate the syringe pump flowrate corresponding to 1000 ppm.

2.6.3. Flash point

All tests were performed using the PMA4 automated closed-cup tester with 45 mL of fuel. This is a deviation from the D93A standard (70 mL fuel) due to the limited availability of POMEs. Tests with 1-pentanol, which has a similar T_{flash} range, showed no difference between 30, 50, and 70 mL tests, indicating that the evaporating fuel reached equilibrium with the air sufficiently rapidly in this volume range as long as the temperature probe was submerged.

2.6.4. Cetane Number

Cetane number was measured using an Advanced Fuel Ignition Delay Analyzer (AFIDA) instrument according to ASTM D8183-18.

3. Results

3.1. Predicted properties of linear and branched POMEs

Sixty-seven POMEs were evaluated including linear structures of backbone length n = 1–7 and alkyl end groups of length C1-C5 as well as structures with isopropyl and isobutyl end groups, and structures with a tertiary alkyl branch of length C1-C4. To illustrate trends in the properties, predicted values of the parameters used in the two screening phases are presented in Table 3 for a subset of structures, the linear POME molecules. Predicted values of Hansen solubility parameters are presented in Fig. 4. Results for all evaluated POMEs are available in Table S1.

3.2. Predicted properties of POME-Diesel blends

To evaluate the performance of POMEs as diesel fuel blendstocks, blending effects must also be considered. The T_{flash}, LHV, and YSI of selected POMEs blended at 10–50% in diesel were estimated to evaluate the potential of these formulations (Table 4). Complete results are available in Table S1.

3.3. Measured properties of POMEs

Measured values for LHV, YSI, T_{flash}, water solubility, and DCN measured in this study are reported in Table 5.

4. Discussion

4.1. Pomes predicted to pass Phase 1 and 2 criteria for diesel blendstocks

Using the predicted property values, the 67 POME candidates were evaluated using Phase 1 and Phase 2 screening criteria (Tables 1 and 2). Ten molecules passed through Phase 1 of the screening process, where the LHV, T_{melt}, and T_{flash} criteria eliminated most candidates (Table S1). Generally, molecules either satisfied the criterion for T_{flash} or for T_{melt}, but not both. Phase 2 of the screening eliminated one additional molecule. All but three POMEs met the criterion for YSI/LHV, while many branched POME structures failed to meet the criterion for environmental impact. All POMEs satisfying the screening criteria (Fig. 5) have backbone length n = 1–2, but a variety of alkyl groups and branched structures are present.

4.2. Effect of molecular structure on predicted POME properties

For a subset of the POMEs, the predicted fuel property results are presented in Table 3, grouped to show trends in backbone length (n = 1–4) and linear or branched end-groups of different sizes (C1–C4). Fig. 6 displays these results in a manner that enables visualization of trends in the properties. For cetane number and YSI, almost all of the structures meet the criteria. The YSI and YSI/LHV increase as end group size and POME backbone length increase. While increased oxygen content generally leads to decreased YSI, higher molecular weight results in increased sooting tendency. Thus, in the case of the POME structures, the higher molecular weight has a more significant impact than the

Table 3
Predicted fuel properties of some pure linear POMEs. Values highlighted in darker orange are more favorable.

Species		LHV (MJ/kg)	YSI	YSI/LHV	T_{boil} (°C)	T_{melt} (°C)	T_{flash} (°C)	DCN	Water Solubility (mg/L)	Bio-degradable?
POME1	MM	23.2	4.5	0.2	48.0	-95.4	-38.9	53.2	1.3E+05	YES
	EE	28.8	14.4	0.5	98.0	-69.5	-4.8	81.5	2.2E+04	YES
	PP	32.0	27.3	0.9	144.4	-44.7	26.9	87.2	2.8E+03	YES
	BB	34.1	40.2	1.2	187.2	-20.9	56.1	99.0	3.0E+02	YES
	PePe	35.5	53.1	1.5	226.4	1.8	82.9	103.3	7.1E+01	YES
POME2	MM	21.2	5.7	0.3	99.0	-63.8	-4.2	79.0	2.8E+05	YES
	EE	25.9	15.6	0.6	145.3	-39.0	27.5	98.9	3.1E+04	YES
	PP	29.0	28.5	1.0	188.0	-15.2	56.7	100.4	3.4E+03	YES
	BB	31.2	41.4	1.3	227.1	7.5	83.3	108.3	3.7E+02	YES
	PePe	32.9	54.3	1.7	262.6	29.1	107.6	110.8	3.8E+01	YES
POME3	MM	20.0	6.9	0.3	146.2	-33.2	34.1	96.9	3.6E+05	NO
	EE	24.1	16.8	0.7	188.8	-9.5	48.7	109.9	3.9E+04	NO
	PP	27.0	29.7	1.1	227.8	13.2	62.7	109.5	4.1E+03	NO
	BB	29.1	42.6	1.5	263.2	34.8	76.1	115.2	4.3E+02	YES
	PePe	30.8	55.5	1.8	295.0	55.3	129.7	116.6	4.4E+01	YES
POME4	MM	19.3	8.1	0.4	189.6	-3.8	57.7	108.3	4.4E+05	NO
	EE	22.9	18.0	0.8	228.5	18.8	84.3	117.6	4.7E+04	NO
	PP	25.5	30.9	1.2	263.9	40.4	108.5	116.2	4.8E+03	NO
	BB	27.6	43.8	1.6	295.6	61.0	130.1	120.4	4.9E+02	NO
	PePe	29.2	56.6	1.9	323.7	80.4	149.3	121.1	5.0E+01	NO
POME5	MM	18.8	9.3	0.5	229.3	24.5	84.8	116.2	5.3E+05	NO
	MB	23.2	27.2	1.2	280.8	56.5	120.0	121.2	1.7E+04	NO
	BB	26.3	38.5	1.5	324.2	86.1	149.7	124.6	5.6E+02	NO
POME6	MM	18.4	10.5	0.6	265.2	51.8	109.4	122.0	6.1E+05	NO
	MB	22.4	28.3	1.3	311.2	82.1	140.8	125.5	2.0E+04	NO
	BB	25.3	46.2	1.8	349.2	110.1	166.7	127.9	6.3E+02	NO
POME7	MM	18.1	42.3	2.3	297.3	77.9	131.3	126.5	7.0E+05	NO

Greatly Exceeds Criteria — Does not meet Criteria

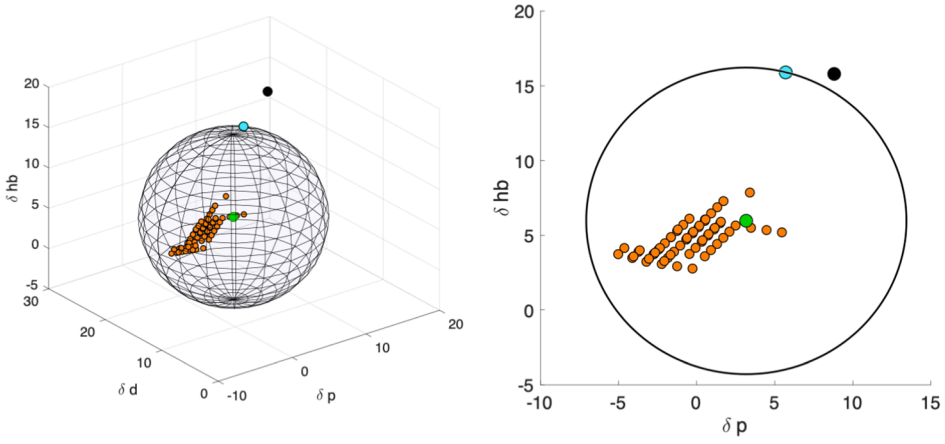

Fig. 4. Hansen solubility diagram showing the Hansen solubility parameters for all 67 POMEs (orange) relative to conventional diesel fuel [50] (green). The radius of the sphere of solubility was determined from the Hansen solubility parameters of n-butanol [50] (blue). Ethanol [50] (black), which is known to have very poor solubility in diesel fuel, is outside of the identified sphere of solubility. (For interpretation of the references to colour in this figure legend, the reader is referred to the web version of this article.)

higher oxygen content. LHV, which is generally low for all POME molecules, decreases as backbone length (and oxygen content) increases, resulting in an inversely proportional increase in the YSI/LHV ratio. There is an incremental increase in the predicted LHV for each $POME_n$ chain length when the end group size increases, attributed to increasing the hydrocarbon-like attribute of the molecule. A similar trend with end group size was observed for T_{flash}, which increased significantly with increasing backbone length. The extremely low flash points of shorter POMEs could present a safety hazard. The property that most notably suffers from increasing backbone length is T_{melt}, with longer POMEs being solids at room temperature.

A marked reduction in water solubility was observed with increased end-group size for each backbone length, consistent with a hypothesis that larger end-groups would increase the hydrophobicity of the molecule and lead to a lower water solubility (Fig. 6). Increased molecular weight, whether from increased backbone length or increased end group

Table 4
Blend properties for 10% and 50% POME-diesel blends of POMEs passing both screening phases. Results for intermediate blends are in Table S1.

Species		LHV		$T_{flash,\ mix}$		YSI	
		10 vol %	50 vol %	10 vol %	50 vol %	10 mol %	50 mol %
$POME_1$	BB	41.9	38.4	88.9	66.1	223.0	136.8
	1P–PP	42.0	38.8	93.7	71.7	224.8	141.8
$POME_2$	PP	41.4	35.9	89.5	66.7	222.0	131.2
	EB	41.4	35.9	89.5	66.7	222.0	131.2
	PB	41.5	36.5	100.0	80.4	224.3	138.9
	iBiB	41.6	37.0	98.2	77.7	227.5	151.7
	1P–PM	41.5	36.5	94.1	72.2	224.0	137.2
	1E–PP	41.6	37.0	103.0	85.4	225.9	143.7
	1 M – BP	41.6	37.0	103.0	85.4	225.9	143.7

Table 5
Measured POME properties.

Species		LHV (MJ/kg)	YSI	T_{flash} (°C)	DCN	Water Solubility (mg/L)
$POME_1$	MM	20.62	8.1 ± 5			387000 ± 18
$POME_1$	EE	27.80	15.5 ± 5	< 0		68500 ± 5
$POME_1$	PP		30.8 ± 5	33.4 ± 0.5	53.6 ± 0.4	3870 ± 0.6
$POME_1$	BB	33.82	44.8 ± 5	59.9 ± 1.1	74.7 ± 0.6	130 ± 05
$POME_3$	MM	19.78	2.8 ± 5	48.2 ± 0.3		421000 ± 29
$POME_4$	MM	19.6		85.6 ± 0.4		543000 ± 74
$POME_5$	MM	18.8		114.8 ± 1.2		442000 ± 40

size, led to higher T_{boil}.

POMEs with branched end-groups showed comparable predicted fuel property trends to those shown in Figs. 6 and 7 for their linear counterparts with similar oxymethylene backbone lengths. Branched POMEs had similar predicted LHV as their linear analogs (same oxymethylene backbone and end groups) at the cost of higher YSI that resulted in increased predicted YSI/LHV ratios at longer backbones. Branched POMEs also had slightly lower boiling points and higher water solubility than their linear equivalents despite having similar molecular weight.

The importance of the end-group structure on small chain length POMEs, where the end-group makes up a larger portion of the overall structure, is exemplified by comparing the values for $POME_1$ and $POME_2$ molecules. For $POME_1$ molecules, the cetane number, LHV, T_{flash}, and water solubility values all improve upon exchange from MM to larger groups; in the case of LHV, T_{flash}, and water solubility, larger end groups result in the POME having property values that meet the criteria. Importantly, the calculated YSI values of all BB-$POME_n$ remain markedly below the 246 value for conventional diesel fuel. Similar improvements were observed for $POME_2$, where PP and BB structures, along with their branched counterparts, meet the criteria for nearly all the properties.

It is helpful to identify indices for describing the molecules in terms of their oxymethylene backbones and alkyl end groups so that linear and branched structures can be compared directly and so that the contributions of these structures to POME properties can be described. Here, the Alkyl Index (AI) is defined as the total number of carbon atoms making up the alkyl end groups and tertiary alkyl branch of a POME. The Oxymethylene Index (OI) gives the number of oxygen atoms contained in oxymethylene backbone. The ratio of these indices can also be a helpful descriptor, as it indicates the extent to which the oxymethylene or alkyl structures dominate the overall molecular structure of a POME. This ratio, given by the oxymethylene index divided by the alkyl index, is called the O/A ratio.

To understand the effect of branching, branched and linear POMEs across a range of O/A ratios (0.25–4) were compared (Fig. 7). While there is not a defined trend between O/A ratio and values of YSI, CN, T_{flash}, T_{boil} and T_{melt}, lower O/A ratios (<1) favor higher LHV and lower water solubility across different POME lengths and linear or branched structures. This relationship is of great value since LHV and water solubility are the two fuel properties in which most POMEs are deficient. In a comparison of POMEs with the same OI and AI values but different branching (Table S2), the effect of branching on YSI is unclear, as some pairs show increased YSI with branching, while other pairs demonstrate lower YSI with branching. Values of T_{boil} and T_{melt} are affected favorably by branching, while T_{flash} is reduced. Most notably, branched structures are predicted to be recalcitrant to biodegradation. However, due to the lack of measurements for these modified POME structures, the predictive tools used in this study may not fully capture the effects of branching on these properties.

4.3. Blending effects

The LHV, YSI, and T_{flash} of 10, 20, 30, 40, and 50% blends of POMEs in diesel fuel were predicted (Table S1). Blend properties are important to consider since POMEs will ultimately be used as diesel blendstocks.

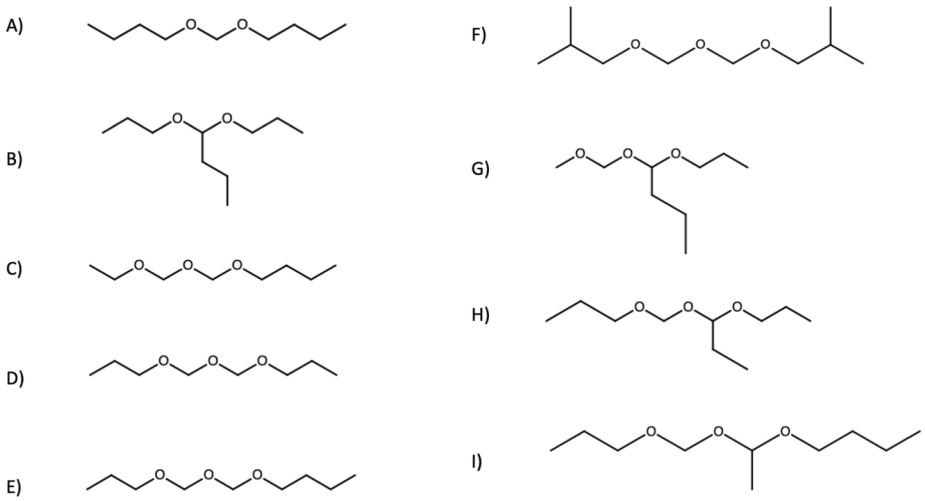

Fig. 5. POMEs that passed Phases 1 and 2 of screening. A) BB-$POME_1$, B) 1P-PP $POME_1$, C) EB-$POME_2$, D) PP-$POME_2$, E) PB-$POME_2$, F) iBiB-$POME_2$, G) 1P-PM-$POME_2$, H) 1E-PP-$POME_2$, I) 1 M-BP-$POME_2$.

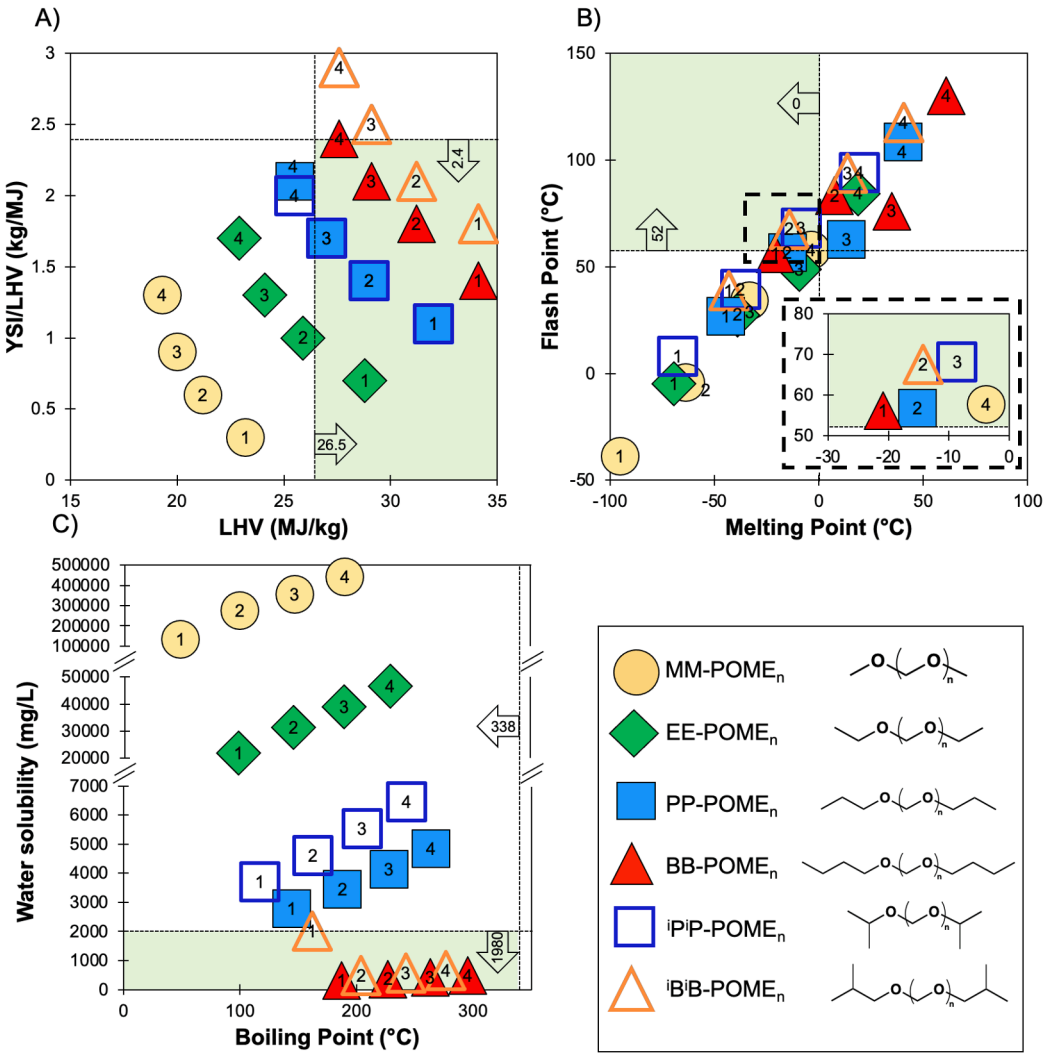

Fig. 6. Relationships among predicted fuel properties and structures of linear POME$_n$ (n = 1–4) with linear and branched end groups (C1–C4). The screening criteria from Tables 1 and 2 are represented by dotted lines and targets are highlighted in light green. A) YSI/LHV and LHV, B) T_{flash} and T_{melt}, C) water solubility and T_{boil}. Numeration within the same marker type indicate the POME$_n$ chain length. (For interpretation of the references to colour in this figure legend, the reader is referred to the web version of this article.)

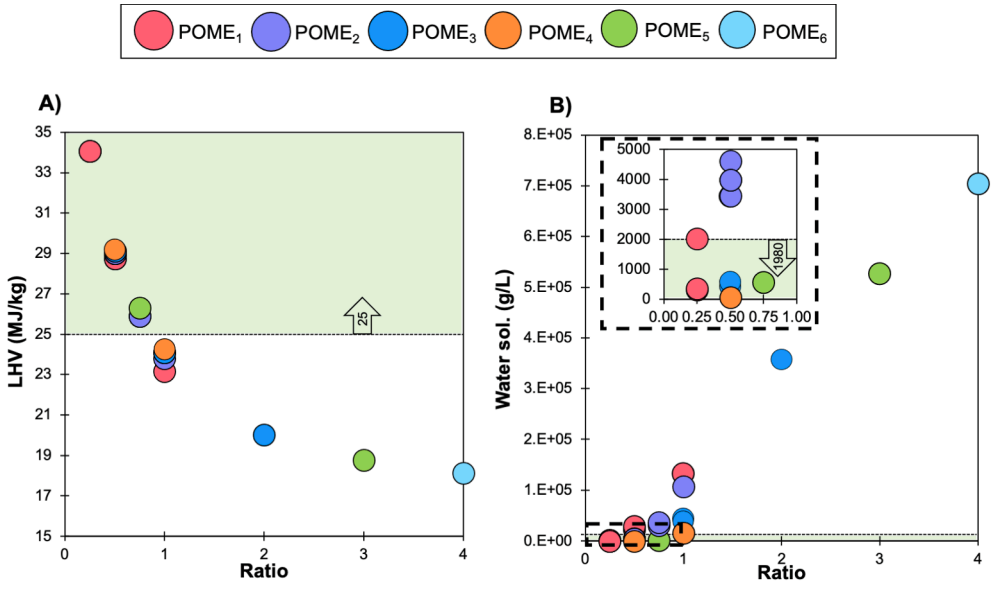

Fig. 7. Relationships between A) LHV and B) water solubility with O/A ratio for linear POME structures. Dotted lines in B) show the region enlarged in the inset plot. The requirements of the screening criteria from Tables 1 and 2 are indicated by arrows that point to the fuel property improvement direction and targeted areas highlighted in light green. (For interpretation of the references to colour in this figure legend, the reader is referred to the web version of this article.)

POMEs that passed through the screening are all predicted to have the potential to be blended at fractions as high as 50% and still meet LHV and T_{flash} criteria (Table 4). We note that the blending models implemented in this study are all based on ideal, linear blending behavior, which may not apply to POME-diesel blends. However, linear blending models have provided accurate estimates of blend properties for other oxygenated blendstocks, including LHV, density, and T_{flash} for biodiesel-diesel blends [52,53] and YSI for ethanol-gasoline [54]. Thus, there is support for the use of linear models as a first-order estimate of blend properties.

4.4. Evaluation of predictive models

Measured data were used to evaluate the accuracy of the employed predictive tools for evaluating POMEs (Tables 6 and 7). There are expected sources of error for each predictive model used. Models that only account for elemental mass fractions, such as those used to predict LHV, do not account for chemical groups or structural variations. These models are typically developed for a specific class of molecules and are not as accurate when applied to new structures. For example, the Dulong and Boie models used (Eqn. (5) and (6)) in this study were developed for the analysis of coal [38].

Slightly more robust are group contribution methods. These models are designed to be applicable to multiple classes of molecules and account for chemical groups and differing structures. However, since POMEs, and the modified POMEs explored here, are novel molecules, group contribution methods are less able to properly account for these POME structures. The model used in this study for the calculation of ignition delay and DCN was developed for oxygenated hydrocarbons; however, because POMEs were not present in the training data, some amount of error is expected. A numerical issue arose in use of Eq. (10), since DCN cannot be calculated for molecules with predicted ignition delays shorter than 1.512 ms. While POMEs are expected to have extremely short ignition delays, a new method for the prediction of DCN of POMEs would be beneficial. A group contribution method was also used for the estimation of POME solubility in diesel fuels. This method, while seemingly versatile, accounted poorly for POME structures. Although DMM is included in the training data for this method, and even appears as a secondary structure in the second-order groups, there is no way to consistently account for the structures of POMEs with longer backbones. The database for the group contribution model used to predict YSI contained three POME structures (MM-$POME_1$, EE-$POME_1$, BB-$POME_1$) on the date of accession [60]. Only POMEs with backbone length n = 1 were included in this set, so the model may fail to extrapolate accurately to longer POME structures.

Machine learning models, such as that used for the prediction of DCN, can be powerful tools when the training data includes sufficient information to capture the behavior of a given class of molecules. Machine learning model fitness depends heavily on the size of the training data set, and while several similar structures, such as triethylene glycol monomethyl ether, were included in the training data, no POMEs were used.

Table 7
Statistical evaluation of models used in this work by comparing predicted (Table 3) vs. measured (Table 6) values.

Property	Model	Average Error	RMSE	R^2
T_{boil}	Adapted Stein and Brown	6.8%	8.84	0.986
T_{melt}	Mean or Weighted T_{melt}	9.1%	8.41	0.983
T_{flash}	Butler (Eqn. (1))	22%	16.8	0.963
T_{flash}	Prugh (Eqn. (2))	59%	32.8	0.991
T_{flash}	Prugh Alcohols (Eqn. (3))	24%	13.5	0.992
LHV	Dulong (Eqn. (5))	4.9%	1.19	0.967
LHV	Boie (Eqn. (6))	4.3%	0.99	0.971
LHV	Lloyd and Davenport (Eqn. (7))	2.7%	0.97	0.969
DCN	Machine learning model	43%	30.4	0.45
DCN	Group contribution model	240%	387	0.46
YSI	Group contribution model	44%	3.59	0.973
Water Solubility	Octanol/water partition coefficient	50%	112,000	0.80

Average error and root mean square error (RMSE) were used to evaluate each model (Table 7). The R^2 values for the linear regression of predicted vs. measured values are also presented in Table 7. While a high R^2 value does not necessarily reflect the accuracy of a model, it provides insight to the relationship between a model's predictors and resulting property estimations. For example, the linear regression of predicted vs. measured values for the Prugh model (Eqn. (2)) has the highest R^2 value of the T_{flash} models, yet it has the highest average error (Fig. 8). This implies that the Prugh model is a strong predictor of T_{flash} for POMEs but has a highly consistent error. In this case, the Prugh model consistently predicts the T_{flash} at an average of 32.4 °C lower than measured. If that were true for all of the POME T_{flash} predictions, only five candidates would pass both screening phases. Similar analyses of predicted vs. measured values for the other properties were also developed (Figs. S1–S5).

5. Conclusions

In this study, the fuel properties of 67 POMEs were predicted and used to identify promising diesel blendstock candidates. Nine POMEs are predicted to have structures that provide for substantial reduction in soot emissions compared to conventional diesel fuel while retaining or improving fuel properties appropriate for blending in diesel. Short chain length POMEs (OI = 1–2) and AI 6–8 appear to be most promising, with all nine identified POMEs belonging to this subset of POME structures. Further studies are necessary to assess the validity of structure–activity models for branched POME structures, as branching would likely have effects not captured by these models.

The models used in these predictions were shown to have a wide range of accuracy and those predictive tools should be revised by incorporation of POME measurements. In some cases, such as for LHV and T_{boil}, existing models provided highly accurate predictions despite

Table 6
Measured POME properties used to evaluate models. Values not marked with a citation were determined in this study (Table 5).

Species		T_{boil} (°C)	T_{melt} (°C)	T_{flash} (°C)	LHV (MJ/kg)	DCN	YSI	Water Solubility (mg/L)
$POME_1$	MM	42.3 [61]	−105 [61]	−32 [61]	20.62	50 [61]	8.1	387,000
$POME_1$	EE	88 [61]	−66 [61]		27.8	47 [26]	15.5	68,500
$POME_1$	PP			33.4		53.6	30.8	3870
$POME_1$	BB			59.9	33.8	74.7	44.8	130
$POME_2$	MM	105 [62]	−70 [62]			68 [26]		
$POME_2$	EE	140 [63]	−45 [26]	36 [26]	25.7 [26]	63[26]		
$POME_3$	MM	155.9 [62]	−43 [62]	48.2	19.78	72 [26]	2.8	421,000
$POME_3$	EE	185 [63]	−24 [26]	68 [26]	23.7 [26]	67 [26]		
$POME_4$	MM	201.8 [62]	−10 [62]	85.6	19.6	84 [26]		543,000
$POME_4$	EE			95 [26]	19.6	70 [26]		
$POME_5$	MM	242.4 [62]	18 [62]	115	18.8	93 [26]		442,000

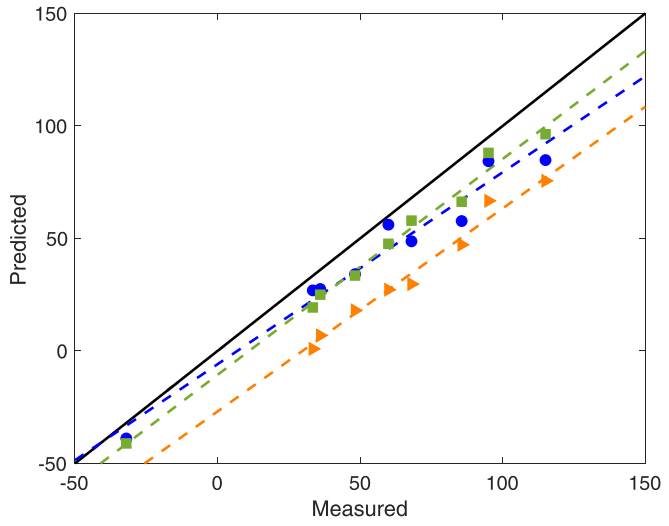

Fig. 8. Predicted vs. measured values for T_{flash}. Solid black line: predicted = measured. Blue circles: Butler model (Eqn. (1)) predictions vs. measured data. Orange triangles: Prugh model (Eqn. (2)) predictions vs. measured data. Green squares: Prugh Alcohol model (Eqn. (3)) vs. measured data. Dotted blue line: linear regression of predicted vs. measured values for the Butler model. Dotted orange line: linear regression of predicted vs. measured values for the Prugh model. Dotted green line: linear regression of predicted vs. measured values for the Prugh Alcohol model. (For interpretation of the references to colour in this figure legend, the reader is referred to the web version of this article.)

having no POME structures in the training data. The finding that some models have high R^2 values and high error, such that they consistently overestimate or underestimate property values, could be used to propose a more accurate versions of those models for use with POMEs.

We note that the screening of POME structures was based on pure component values rather than on the properties of their blends with diesel. Considering that POMEs will be used in blends, it may also be reasonable to relax certain screening criteria. This would allow consideration of additional molecules that did not pass the original screening criteria but might have other advantages, such as ease of synthesis. As examples, PePe-$POME_1$, PB-$POME_1$, MP-$POME_2$, and EP-$POME_2$ all pass environmental screening and would pass through a slightly relaxed fuel property screen. Generally, POMEs with an O/A ratio of 0.2–0.6 may be viable diesel blendstocks.

Many of the POMEs identified in this work have yet to be synthesized, and most have not been produced on an industrial scale. Future research should focus on improving the synthesis of promising POMEs identified in this study and experimentally determining the performance of those molecules in diesel blends.

Declaration of Competing Interest

The authors declare that they have no known competing financial interests or personal relationships that could have appeared to influence the work reported in this paper.

Acknowledgements

This work was supported in part by the U.S. Department of Energy's Office of Energy Efficiency and Renewable Energy (EERE) under the Bioenergy Technologies Office, Co-Optimization of Fuels and Engines Initiative award number DE-EE0008726. Also, this work was authored in part by the National Renewable Energy Laboratory, operated by Alliance for Sustainable Energy, LLC, for the U.S. Department of Energy (DOE) under Contract Nos. DE-AC36-08GO28308. This research was conducted as part of the Co-Optimization of Fuels & Engines (Co-Optima) project sponsored by the U.S. Department of Energy – Office of Energy Efficiency and Renewable Energy, Bioenergy Technologies and Vehicle Technologies Offices. Co-Optima is a collaborative project of several national laboratories initiated to simultaneously accelerate the introduction of affordable, scalable, and sustainable biofuels and high-efficiency, low-emission vehicle engines. The views expressed in this article do not necessarily represent the views of the DOE or the U.S. Government. The U.S. Government retains and the publisher, by accepting the article for publication, acknowledges that the U.S. Government retains a nonexclusive, paid-up, irrevocable, worldwide license to publish or reproduce the published form of this work, or allow others to do so, for U.S. Government purposes.

The authors thank Gina Fioroni and Cameron Hays of the Catalytic Carbon Transformation & Scale-up Center at the National Renewable Energy Laboratory for assistance with cetane number measurements.

Appendix A. Supplementary data

Supplementary data to this article can be found online at https://doi.org/10.1016/j.fuel.2021.120509.

References

[1] Naber JD, Johnson JE. Internal combustion engine cycles and concepts. In: Woodhead Publishing; 2014. p. 197–224. https://doi.org/10.1533/9780857097422.2.197.
[2] Jacobson MZ. Short-term effects of controlling fossil-fuel soot, biofuel soot and gases, and methane on climate, Arctic ice, and air pollution health. J Geophys Res 2010;115:D14209. https://doi.org/10.1029/2009JD013795.
[3] Polichetti G, Cocco S, Spinali A, Trimarco V, Nunziata A. Effects of particulate matter (PM10, PM2.5 and PM1) on the cardiovascular system. Toxicology 2009; 261(1-2):1–8. https://doi.org/10.1016/j.tox.2009.04.035.
[4] Watkinson WP, Campen MJ, Nolan JP, Costa DL. Cardiovascular and systemic responses to inhaled pollutants in rodents: effects of ozone and particulate matter. Environ Health Perspect 2001;109(suppl 4):539–46. https://doi.org/10.1289/ehp.01109s4539.
[5] Zelikoff JT, Chen LC, Cohen MD, Fang K, Gordon T, Li Y, et al. Effects of Inhaled Ambient Particulate Matter on Pulmonary Antimicrobial Immune Defense. Inhal Toxicol 2003;15(2):131–50. https://doi.org/10.1080/08958370304478.
[6] Bond TC, Doherty SJ, Fahey DW, Forster PM, Berntsen T, DeAngelo BJ, et al. Bounding the role of black carbon in the climate system: A scientific assessment. J Geophys Res Atmos 2013;118(11):5380–552. https://doi.org/10.1002/jgrd.50171.
[7] Afshin A, Sur PJ, Fay KA, Cornaby L, Ferrara G, Salama JS, et al. Health effects of dietary risks in 195 countries, 1990–2017: a systematic analysis for the Global Burden of Disease Study 2017. Lancet 2019;393(10184):1958–72. https://doi.org/10.1016/S0140-6736(19)30041-8.
[8] Burnett R, Chen H, Szyszkowicz M, Fann N, Hubbell B, Pope CA, et al. Global estimates of mortality associated with long-term exposure to outdoor fine particulate matter. Proc Natl Acad Sci 2018;115(38):9592–7. https://doi.org/10.1073/pnas.1803222115.
[9] Ren Yi, Huang Z, Miao H, Di Y, Jiang D, Zeng Ke, et al. Combustion and emissions of a DI diesel engine fuelled with diesel-oxygenate blends. Fuel 2008;87(12): 2691–7. https://doi.org/10.1016/j.fuel.2008.02.017.
[10] Charles K. Westbrook, William J. Pitz A, Curran HJ. Chemical Kinetic Modeling Study of the Effects of Oxygenated Hydrocarbons on Soot Emissions from Diesel Engines† 2006. https://doi.org/10.1021/JP056362G.
[11] Vijayashree P, Ganesan V. Oxygenated Fuel Additive Option for PM Emission Reduction from Diesel Engines—A Review, Springer. Singapore 2019:141–63. https://doi.org/10.1007/978-981-13-3299-9_7.
[12] Hansen AC, Zhang Q, Lyne PWL. Ethanol–diesel fuel blends — a review. Bioresour Technol 2005;96:277–85. https://doi.org/10.1016/J.BIORTECH.2004.04.007.
[13] Arcoumanis C, Bae C, Crookes R, Kinoshita E. The potential of di-methyl ether (DME) as an alternative fuel for compression-ignition engines: A review. Fuel 2008; 87(7):1014–30. https://doi.org/10.1016/j.fuel.2007.06.007.
[14] McEnally CS, Pfefferle LD. The effects of dimethyl ether and ethanol on benzene and soot formation in ethylene nonpremixed flames. Proc Combust Inst 2007;31 (1):603–10. https://doi.org/10.1016/j.proci.2006.07.005.
[15] Burke SC, Ratcliff M, McCormick R, Rhoads R, Windom B. Distillation-based Droplet Modeling of Non-Ideal Oxygenated Gasoline Blends: Investigating the Role of Droplet Evaporation on PM Emissions. SAE Int J Fuels Lubr 2017;10(1):69–81. https://doi.org/10.4271/2017-01-0581.
[16] Miyamoto N, Ogawa H, Nurun NM, Obata K, Arima T. Smokeless, Low NOx, High Thermal Efficiency, and Low Noise Diesel Combustion with Oxygenated Agents as Main Fuel on JSTOR. SAE Trans 1998;107:171–7.
[17] McEnally CS, Pfefferle LD. Sooting Tendencies of Oxygenated Hydrocarbons in Laboratory-Scale Flames. Environ Sci Technol 2011;45(6):2498–503. https://doi.org/10.1021/es103733q.

[18] He B-Q, Shuai S-J, Wang J-X, He H. The effect of ethanol blended diesel fuels on emissions from a diesel engine. Atmos Environ 2003;37(35):4965–71. https://doi.org/10.1016/j.atmosenv.2003.08.029.

[19] Paul J. Squillace, John S. Zogorski, William G. Wilber A, Price C V. Preliminary Assessment of the Occurrence and Possible Sources of MTBE in Groundwater in the United States, 1993−1994 1996. https://doi.org/10.1021/ES9507170.

[20] US EPA. Overview | Methyl Tertiary Butyl Ether (MTBE) | US EPA 2016. https://archive.epa.gov/mtbe/web/html/faq.html (accessed April 27, 2020).

[21] Sun R, Delidovich I, Palkovits R. Dimethoxymethane as a Cleaner Synthetic Fuel: Synthetic Methods. Catalysts, Reaction Mech 2019;9(2):1298–318. https://doi.org/10.1021/acscatal.8b04441.

[22] Burger J, Siegert M, Ströfer E, Hasse H. Poly(oxymethylene) dimethyl ethers as components of tailored diesel fuel: Properties, synthesis and purification concepts. Fuel 2010;89(11):3315–9. https://doi.org/10.1016/j.fuel.2010.05.014.

[23] Ouda M, Yarce G, White RJ, Hadrich M, Himmel D, Schaadt A, et al. Poly (oxymethylene) dimethyl ether synthesis – a combined chemical equilibrium investigation towards an increasingly efficient and potentially sustainable synthetic route. React Chem Eng 2017;2(1):50–9. https://doi.org/10.1039/C6RE00145A.

[24] Schmitz N, Homberg F, Berje J, Burger J, Hasse H. Chemical equilibrium of the synthesis of poly (oxymethylene) dimethyl ethers from formaldehyde and methanol in aqueous solutions. Ind Eng Chem Res 2015;54(25):6409–17. https://doi.org/10.1021/acs.iecr.5b01148.

[25] Zhao Y, Xu Z, Chen H, Fu Y, Shen J. Mechanism of chain propagation for the synthesis of polyoxymethylene dimethyl ethers. J Energy Chem 2013;22(6):833–6. https://doi.org/10.1016/S2095-4956(14)60261-8.

[26] Lautenschütz L, Oestreich D, Seidenspinner P, Arnold U, Dinjus E, Sauer J. Physico-chemical properties and fuel characteristics of oxymethylene dialkyl ethers. Fuel 2016;173:129–37. https://doi.org/10.1016/J.FUEL.2016.01.060.

[27] Gao X-J, Wang W-F, Gu Y-Y, Zhang Z-Z, Zhang J-F, Zhang Q-D, et al. Synthesis of Polyoxymethylene Dimethyl Ethers from Dimethyl Ether Direct Oxidation over Carbon-Based Catalysts. ChemCatChem 2018;10(1):273–9. https://doi.org/10.1002/cctc.v10.110.1002/cctc.201701213.

[28] To AT, Wilke TJ, Nelson E, Nash CP, Bartling A, Wegener EC, et al. Dehydrogenative Coupling of Methanol for the Gas-Phase, One-Step Synthesis of Dimethoxymethane over Supported Copper Catalysts. ACS Sustain Chem Eng 2020;8(32):12151–60. https://doi.org/10.1021/acssuschemeng.0c03606.

[29] Pahima E, Hoz S, Ben-Tzion M, Major DT. Computational design of biofuels from terpenes and terpenoids. Sustain Energy Fuels 2019;3(2):457–66. https://doi.org/10.1039/C8SE00390D.

[30] ASTM International. Standard Test Method for Smoke Point of Kerosene and Aviation Turbine Fuel. 2019.

[31] Das DD, McEnally CS, Kwan TA, Zimmerman JB, Cannella WJ, Mueller CJ, et al. Sooting tendencies of diesel fuels, jet fuels, and their surrogates in diffusion flames. Fuel 2017;197:445–58. https://doi.org/10.1016/j.fuel.2017.01.099.

[32] Dwivedi G, Sharma MP. Impact of cold flow properties of biodiesel on engine performance. Renew Sustain Energy Rev 2014;31:650–6. https://doi.org/10.1016/J.RSER.2013.12.035.

[33] ASTM International. Designation: D975 − 20a Standard Specification for Diesel Fuel 1. 2020. https://doi.org/10.1520/D0975-20A.

[34] Saldana DA, Starck L, Mougin P, Rousseau B, Creton B. Prediction of Flash Points for Fuel Mixtures Using Machine Learning and a Novel Equation. Energy Fuels 2013;27(7):3811–20. https://doi.org/10.1021/ef4005362.

[35] US EPA. Estimation Program Interface Suite for Microsoft® Windows, v 4.11 2012.

[36] Butler RM, Cooke GM, Lukk GG, Jameson BG. Prediction of Flash Points of Middle Distillates. Ind Eng Chem Res 1956;48(4):808–12. https://doi.org/10.1021/ie50556a041.

[37] Prugh RW. Estimation of flash point temperature. J Chem Educ 1973;50(2):A85. https://doi.org/10.1021/ed050pA85.1.

[38] Kraetsch EJ. Application of Dulong's Formula in the Ultimate Analysis of. Coal. 1934.

[39] Boie W. Fuel technology calculations. Energietechnik 1953;3:309–16.

[40] Lloyd WG, Davenport DA. Applying thermodynamics to fossil fuels: Heats of combustion from elemental compositions. J Chem Educ 1980;57(1):56. https://doi.org/10.1021/ed057p56.

[41] Mason DM, Gandhi K. Formulas for calculating the heating value of coal and coal char: development, tests, and uses. Inst Gas Technol 1980.

[42] ASTM International. Standard Test Method for Heat of Combustion of Liquid Hydrocarbon Fuels by Bomb Calorimeter 1. 2019. https://doi.org/10.1520/D0240-19.

[43] Das DD, St. John PC, McEnally CS, Kim S, Pfefferle LD. Measuring and predicting sooting tendencies of oxygenates, alkanes, alkenes, cycloalkanes, and aromatics on a unified scale. Combust Flame 2018;190:349–64. https://doi.org/10.1016/j.combustflame.2017.12.005.

[44] Dahmen M, Marquardt W. A Novel Group Contribution Method for the Prediction of the Derived Cetane Number of Oxygenated Hydrocarbons. Energy Fuels 2015;29(9):5781–801. https://doi.org/10.1021/acs.energyfuels.5b01032.

[45] ASTM International. Standard Test Method for Determination of Ignition Delay and Derived Cetane Number (DCN) of Diesel Fuel Oils by Combustion in a Constant Volume Chamber 1,2. 2019. https://doi.org/10.1520/D6890-18.

[46] Kessler T, Sacia E, Bell A, Fuel JM. Artificial neural network based predictions of cetane number for furanic biofuel additives. Fuel 2017;2017(26):171–9.

[47] St. John PC, Guan Y, Kim Y, Kim S, Paton RS. Prediction of organic homolytic bond dissociation enthalpies at near chemical accuracy with sub-second computational cost. Nat Commun 2020;11(1). https://doi.org/10.1038/s41467-020-16201-z.

[48] McCormick RL, Fioroni G, Fouts L, Christensen E, Yanowitz J, Polikarpov E, et al. Selection Criteria and Screening of Potential Biomass-Derived Streams as Fuel Blendstocks for Advanced Spark-Ignition Engines. SAE Int J Fuels Lubr 2017;10(2):442–60. https://doi.org/10.4271/2017-01-0868.

[49] Stefanis E, Panayiotou C. Prediction of Hansen Solubility Parameters with a new group-contribution method. Int J Thermophys 2008;29(2):568–85. https://doi.org/10.1007/s10765-008-0415-z.

[50] Batista MM, Guirardello R, Krähenbühl MA. Determination of the Hansen Solubility Parameters of Vegetable Oils, Biodiesel, Diesel, and Biodiesel-Diesel Blends. J Am Oil Chem Soc 2015;92(1):95–109. https://doi.org/10.1007/s11746-014-2575-2.

[51] Wickey R, Chittenden D. Flash Points of Blends Correlated. Hydrocarb Process 1963;42:157.

[52] Tesfa B, Gu F, Mishra R, Ball AD. LHV predication models and LHV effect on the performance of CI engine running with biodiesel blends. Energy Convers Manag 2013;71:217–26. https://doi.org/10.1016/J.ENCONMAN.2013.04.005.

[53] Gülüm M, Bilgin A. Density, flash point and heating value variations of corn oil biodiesel–diesel fuel blends. Fuel Process Technol 2015;134:456–64. https://doi.org/10.1016/J.FUPROC.2015.02.026.

[54] McEnally CS, Xuan Y, St. John PC, Das DD, Jain A, Kim S, et al. Sooting tendencies of co-optima test gasolines and their surrogates. Proc Combust Inst 2019;37(1):961–8. https://doi.org/10.1016/j.proci.2018.05.071.

[55] Mueller CJ, Cannella WJ, Bays JT, Bruno TJ, DeFabio K, Dettman HD, et al. Diesel Surrogate Fuels for Engine Testing and Chemical-Kinetic Modeling: Compositions and Properties. Energy Fuels 2016;30(2):1445–61. https://doi.org/10.1021/acs.energyfuels.5b0287910.1021/acs.energyfuels.5b02879.s001.

[56] Aghahossein Shirazi S, Abdollahipoor B, Martinson J, Windom B, Foust TD, Reardon KF. Effects of dual-alcohol gasoline blends on physiochemical properties and volatility behavior. Fuel 2019;252:542–52. https://doi.org/10.1016/j.fuel.2019.04.105.

[57] Chen Z, Liu J, Han Z, Du B, Liu Y, Lee C. Study on performance and emissions of a passenger-car diesel engine fueled with butanol–diesel blends. Energy 2013;55:638–46. https://doi.org/10.1016/J.ENERGY.2013.03.054.

[58] McEnally C, Pfefferle L. Improved sooting tendency measurements for aromatic hydrocarbons and their implications for naphthalene formation pathways. Combust Flame 2007;148(4):210–22. https://doi.org/10.1016/j.combustflame.2006.11.003.

[59] McEnally CS, Das DD, Pfefferle LD. Yield Sooting Index Database Volume 2: Sooting Tendencies of a Wide Range of Fuel Compounds on a Unified Scale - Pfefferle Research Group: Combustion and Nanomaterials Dataverse. Harvard Dataverse 2017. https://dataverse.harvard.edu/dataset.xhtml?persistentId=doi:10.7910/DVN/7HGFT8 (accessed May 18, 2020).

[60] St. John PC, Kairys P, Das DD, McEnally CS, Pfefferle LD, Robichaud DJ, et al. A Quantitative Model for the Prediction of Sooting Tendency from Molecular Structure. Energy Fuels 2017;31(9):9983–90. https://doi.org/10.1021/acs.energyfuels.7b00616.

[61] Lide DR. CRC handbook of chemistry and physics. 93rd ed. 2012.

[62] Boyd RH. Some physical properties of polyoxymethylene dimethyl ethers. J Polym Sci 1961;50:133–41. https://doi.org/10.1002/pol.1961.1205015316.

[63] Marchionna M, Patrini R. Patent Application EP1505049A1, European Patent Office: A process for the selective production of dialkyl-polyformals; 2000.